Biomechanically based simulation of brain deformations for intraoperative image correction: coupling of elastic and fluid models

A. Hagemann, K. Rohr, H. S. Stiehl,

Universität Hamburg, FB Informatik, AB Kognitive Systeme,
Vogt-Kölln-Straße 30, D-22527 Hamburg, Germany

ABSTRACT

In order to improve the accuracy of image-guided neurosurgery, different biomechanical models have been developed to correct preoperative images w.r.t. intraoperative changes like brain shift or tumor resection. All existing biomechanical models simulate different anatomical structures by using either appropriate boundary conditions or by spatially varying material parameter values, while assuming the same physical model for all anatomical structures. In general, this leads to physically implausible results, especially in the case of adjacent elastic and fluid structures. Therefore, we propose a new approach which allows to couple different physical models. In our case, we simulate rigid, elastic, and fluid regions by using the appropriate physical description for each material, namely either the Navier equation or the Stokes equation. To solve the resulting differential equations, we derive a linear matrix system for each region by applying the finite element method (FEM). Thereafter, the linear matrix systems are linked together, ending up with one overall linear matrix system. Our approach has been tested using synthetic as well as tomographic images. It turns out from experiments, that the integrated treatment of rigid, elastic, and fluid regions significantly improves the prediction results in comparison to a pure linear elastic model.

Keywords: biomechanical model, inhomogeneous materials, finite element method, intraoperative image correction, Navier equation, Stokes equation

1. INTRODUCTION

The accuracy of image-guided neurosurgery generally suffers from intraoperative changes of the brain anatomy due to, e.g., tumor resection or brain shift.[1] To improve upon navigation accuracy, a variety of biomechanical models have been developed[2–6] to predict brain deformations and thus to correct the preoperative images w.r.t. surgery induced effects. Other biomechanical models have been described in the context of preoperative planning for registration purposes[7–10] which can be used likewise to predict brain deformations.

All these models simulate the biomechanical behaviour of different anatomical structures by either spatially varying the underlying material parameter values, while assuming the same physical model for all anatomical structures,[7,2,9,10,5,6] or by applying appropriate boundary conditions.[3,4,8] An example for the latter case is the integration of the skull bone or the falx as a non-moving part (known as *homogeneous Dirichlet boundary condition*). However, the existing approaches generally lead to physically inadequate simulations, particularly in the case of combined elastic/fluid regions. For example, in Hagemann *et al.*,[5] where the Navier equation has been used as underlying physical model, the ventricular system was modeled as a rigid object, motivated by the reported incompressibility of cerebrospinal fluid.[11,12] Using this assumption, good registration results are obtained if none of the prescribed correspondences, which drive the deformation of the model, were given in the vicinity of the ventricular system. Otherwise the model gives a poor registration result, leading to an unrealistic deformation of the fluid region as shown in Figure 1. An approach that directly simulates the physical behaviour of inhomogeneous fluids by using the Navier-Stokes equation is the model of Lester *et al.*,[9] which is motivated by the homogeneous fluid model of Christensen *et al.*[13] But in both cases, it is assumed that all anatomical structures behave like fluids which is generally not the case.

Send correspondence to A. Hagemann
E-Mail: hagemann@informatik.uni-hamburg.de Tel.: +49 (40) 42883 2577 Fax: +49 (40) 42883 2572

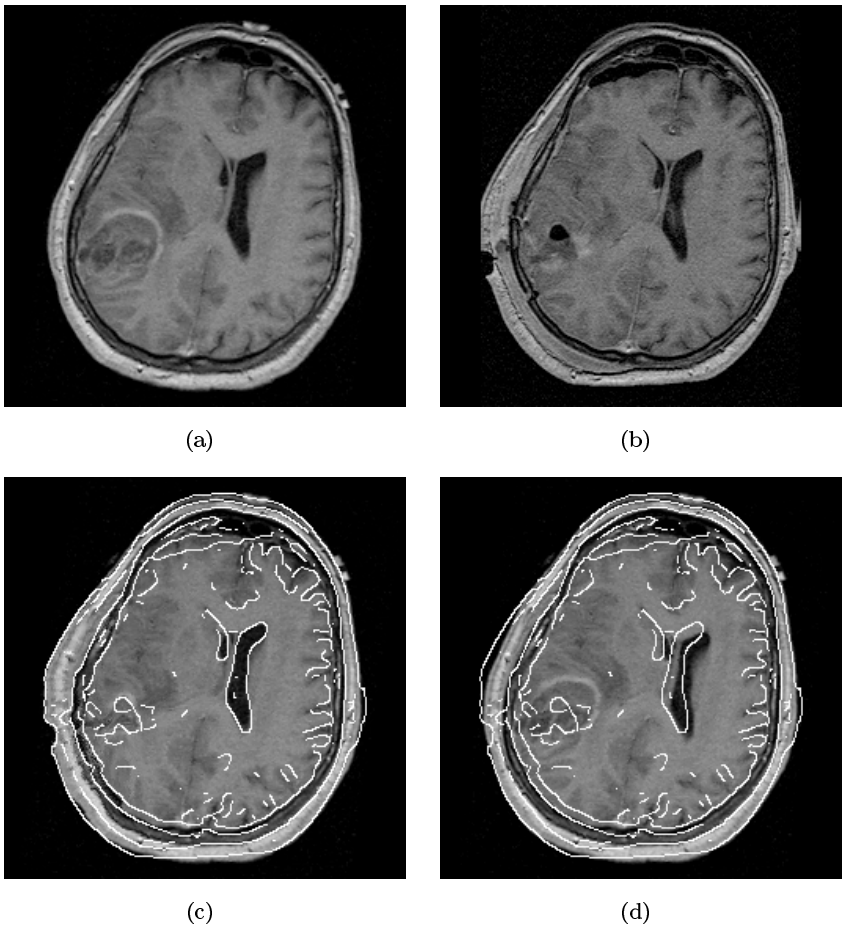

Figure 1. Simulation of fluid parts (ventricular system) while treating them as rigid object surrounded by elastic material: registration result of the preoperative image (a) with the postoperative image (b) while using (c) no correspondences in the vicinity of the ventricular system and (d) while using two parallel correspondences at the contour of the ventricular system, leading to an unrealistic pure translation of this structure. For a better visualization of the result, the edges of the postoperative image (b) have been overlaid on subfigures (c) and (d).

In order to improve the prediction of brain deformations, we extend our biomechanical model[14] to cope with anatomical structures consisting of rigid, elastic, and fluid materials while using the appropriate physical descriptions for each material, namely either the Navier equation or the Stokes equation. Our approach is based on the well-established physical theory of continuum mechanics to handle *inhomogeneous* materials. With this scheme, an inhomogeneous domain is divided into homogeneous regions, each simulating different materials by using the appropriate constitutive equation. To discretize the problem, we apply the finite element method (FEM) to each region, resulting in a set of sparse linear matrix systems. Thereafter, these matrix systems are assembled together into a single overall system of linear equations via appropriate boundary conditions, which establish a physical link between the corresponding regions. Instead of using forces, which are generally difficult to determine from images, we use a set of given correspondences to drive the deformation of the image. In our approach, it is ensured that the prescribed correspondences are exactly fulfilled. Experiments with synthetic as well as real tomographic images have been carried out and the results were compared against a purely linear elastic model with spatially varying material parameter values to assess the physical plausibility of the predicted deformations.

2. APPROACH

To determine the deformation of an inhomogeneous body Ω, the body is divided into a set of homogeneous regions Ω_i in accordance with the underlying anatomical structures. Different material properties are taken into account by

substituting the appropriate constitutive equation, which describes the stress/strain relationship of a region Ω_i, into the equilibrium equations which describe the state of equilibrium between internal and external forces. Denoting with $\boldsymbol{\sigma}$ the *Eulerian stress tensor*, $\mathbf{f}$ the assumed homogeneous body forces, $\mathbf{n}_i$ the unit vector normal to the surface Γ_i, and $\mathbf{g}^i$ the forces acting on Γ_i, the equilibrium equations for a region Ω_i read[15–17]

$$\begin{cases} -\mathrm{div}[\boldsymbol{\sigma}] = \mathbf{f} & \text{in } \Omega_i \\ \boldsymbol{\sigma}\,\mathbf{n}_i = \mathbf{g}^i & \text{on } \Gamma_i. \end{cases} \tag{1}$$

After substitution of either *Hooke's law* or the *Navier-Poisson law* as appropriate constitutive equations into the equilibrium equations, we get the *Navier equation*

$$(\lambda + \mu)\nabla\mathrm{div}[\mathbf{u}] + \mu\nabla^2\mathbf{u} + \mathbf{f} = \mathbf{0} \tag{2}$$

for the simulation of rigid and elastic materials and the *Stokes equation*

$$-\nabla p + \mu^\star\nabla^2\mathbf{v} + \mathbf{f} = \mathbf{0} \tag{3}$$

to simulate the behaviour of *incompressible* fluids, respectively. Here, ∇ denotes the common Nabla operator, λ and μ the Lamé constants, $\mathbf{u}$ the unknown displacement vector field, p the unknown scalar pressure function, $\mu^\star$ the viscosity parameter, and $\mathbf{v}$ the unknown velocity vector field. Our usage of the Stokes equation, motivated by the reported incompressibility of cerebrospinal fluid,[11,12] is in contrast to Christensen *et al.*[13] or Lester *et al.*[9] where the Navier-Stokes equation has been used to simulate *compressible* fluids and to Edwards *et al.*[18] where the fluid region is allowed to deform almost freely.

According to the additional unknown pressure function p, the Stokes equation, defining a *saddlepoint problem*,[19] cannot be solved alone. Instead, the continuity equation

$$\mathrm{div}\,[\mathbf{v}] = 0, \tag{4}$$

expressing the conservation of mass,[16,20] has to be solved simultaneously. Thereafter, the associated displacement vector field $\mathbf{u}$ of an incompressible fluid can be determined by calculating the total derivative of the velocity vector field w.r.t. time, also known as calculation of the *material derivative*.[16] But the formal restriction of the resulting body deformation being infinitesimal, as implicitly done when using the Navier equation to simulate rigid and elastic materials, allows a simple approximation of the displacement vector field $\mathbf{u}$ by multiplication of the velocity vector field $\mathbf{v}$ with a small time interval dt, i.e.[20]

$$\mathbf{u} = \mathbf{v}dt. \tag{5}$$

Substitution of (5) into the Stokes equation and the continuity equation gives

$$\begin{aligned} -\nabla p + \mu^\star dt^{-1}\nabla^2\mathbf{u} + \mathbf{f} &= \mathbf{0} \\ \mathrm{div}[\mathbf{u}] &= 0 \end{aligned} \tag{6}$$

which can be directly solved for the unknown displacement vector field $\mathbf{u}$. The combined parameter $\mu^\star dt^{-1}$ has now the physical unit of a pressure.

In order to solve the Navier and Stokes equations within sufficiently smooth function spaces, the *method of weighted residuals*[21] is applied. With this method, we demand that the projection of the residuum onto arbitrary weighting functions of the underlying function space vanishes over each corresponding region Ω_i. Using $\mathbf{w}$ and q as arbitrary weighting functions and denoting with $(\cdot,\cdot)$ the common inner product leads to

$$\begin{aligned} \int_{\Omega_i} \left(-\nabla p + \mu^\star dt^{-1}\nabla^2\mathbf{u} + \mathbf{f}, \mathbf{w}\right) d\Omega_i = 0 \\ \int_{\Omega_i} q\,\mathrm{div}[\mathbf{u}]\,d\Omega_i = 0, \end{aligned} \tag{7}$$

for the Stokes equation, while the formulation for the Navier equation is given elsewhere.[5,14] Note, that the continuity equation is satisfied here in a weak sense only, i.e. the solution does not satisfy the incompressibility

constraint pointwise but in the mean, thus leading to the so-called *non-conforming finite element method*.[22,23,19] It can be shown, however, that each classical solution of (7), i.e. a solution satisfying $\mathbf{u} \in C^2(\Omega_i) \cap C^0(\bar{\Omega}_i)$ and $p \in C^1(\bar{\Omega}_i)$ with $\bar{\Omega}_i$ being the closure of Ω_i, is still a classical solution of the Stokes problem (3) satisfying the incompressibility constraint (4).[23,19] Using the Jacobian matrix $\mathbf{J}(\cdot)$, equation (7) can be further transformed into

$$\int_{\Omega_i} -p\,\mathrm{div}[\mathbf{w}] + \mu^\star dt^{-1}\,(J(\mathbf{u}), J(\mathbf{w}))\,d\Omega_i = \int_{\Omega_i} (\mathbf{f}, \mathbf{w})\,d\Omega_i - \int_{\Gamma_i} (\mathbf{w}, p\mathbf{n}_i)\,d\Gamma_i + \int_{\Gamma_i} \mu^\star \left(dt^{-1}\mathbf{J}(\mathbf{u})\mathbf{n}_i, \mathbf{w}\right) d\Gamma_i \tag{8}$$

$$\int_{\Omega_i} q\,\mathrm{div}[\mathbf{u}]\,d\Omega_i = 0. \tag{9}$$

Considering the first boundary integral appearing on the righthand side of (8) reveals that the term $p\mathbf{n}_i$ represents a pressure load[17] $\mathbf{g}^i$ acting on the surface Γ_i. Furthermore, we assume that the fluid must not penetrate the adjacent regions Ω_j which is in accordance with the barrier between cerebrospinal fluid and brain tissue. Mathematically, this requires that the velocity component of the fluid normal to the surface Γ_i vanishes,[20] i.e.

$$\mathbf{J}(\mathbf{v})\mathbf{n}_i = dt^{-1}\mathbf{J}(\mathbf{u})\mathbf{n}_i = \mathbf{0} \qquad \forall \mathbf{x} \in \Gamma_i \tag{10}$$

must hold. This condition is also known as *no-penetration boundary condition*.[20]

By application of the Galerkin method, i.e. taking only finite dimensional subspaces of the underlying vector spaces, spanned by a finite number of basis functions, respectively, all functions can be approximated as finite sums of basis functions multiplied with unknown coefficients. As a result, we can write the Stokes equation in conjunction with the continuity equation as well as the corresponding expression for the Navier equation[5,14] in compact matrix notation thus giving a linear matrix system for each region Ω_i:

$$\mathbf{A}^i\mathbf{u}^i = \mathbf{f} + \mathbf{g}^i. \tag{11}$$

The matrix $\mathbf{A}^i$ is commonly known as *stiffness matrix*, while the vector $\mathbf{u}^i$ contains the unknown pressure/displacement coefficients, $\mathbf{f}$ are the homogeneous body force coefficients, and $\mathbf{g}^i$ are the coefficients of the surface forces acting on Γ_i.

So far, each linear equation system (11) contains the physical description for a homogeneous region Ω_i only. But all matrix systems can be physically linked by applying the *compatibility* and *equilibrium* boundary conditions[24,20]: The former condition states, that the displacements $\mathbf{u}_\Gamma^{ij}$ at the common boundary Γ_{ij} between, e.g., two subregions Ω_i and Ω_j must be equal, while the latter one states that in the equilibrium, the sum of all stress vectors $\mathbf{g}^i$ and $\mathbf{g}^j$ acting on the boundary Γ_{ij} must be zero. Introduction of these boundary conditions and assuming homogeneous body forces $\mathbf{f}$ over $\Omega = \Omega_i \cup \Omega_j$ allows to couple both linear systems, ending up with one overall system of linear equations:

$$\underbrace{\begin{pmatrix} \mathbf{A}_{\Omega\Omega}^i & \mathbf{A}_{\Omega\Gamma}^i & \mathbf{0} \\ \mathbf{A}_{\Gamma\Omega}^i & \mathbf{A}_{\Gamma\Gamma}^i + \mathbf{A}_{\Gamma\Gamma}^j & \mathbf{A}_{\Gamma\Omega}^j \\ \mathbf{0} & \mathbf{A}_{\Omega\Gamma}^j & \mathbf{A}_{\Omega\Omega}^j \end{pmatrix}}_{\mathbf{A}} \underbrace{\begin{pmatrix} \mathbf{u}_\Omega^i \\ \mathbf{u}_\Gamma^{ij} \\ \mathbf{u}_\Omega^j \end{pmatrix}}_{\mathbf{u}} = \underbrace{\begin{pmatrix} \mathbf{f} + \mathbf{g}^i \\ \mathbf{f} \\ \mathbf{f} + \mathbf{g}^j \end{pmatrix}}_{\mathbf{b}}. \tag{12}$$

With $\mathbf{A}_{\Omega\Omega}^i$ etc., we denoted the submatrices of the corresponding stiffness matrices $\mathbf{A}^i$ and $\mathbf{A}^j$ for the subregions Ω_i and Ω_j, respectively. An index including Γ, as appearing in $\mathbf{A}_{\Omega\Gamma}^i$ etc., indicates those submatrices which comprise finite elements belonging to the common boundary Γ_{ij} between both regions. Based on (12) we are able to simulate the physical deformation behaviour of an inhomogeneous body comprising rigid, elastic, and fluid parts.

Special care has to be taken concerning the choice of the finite elements. Due to the incompressibility constraint (4), it is not sufficient for fluid regions to use mixed finite elements with a simple linear displacement approximation and a constant pressure approximation, because the *Babuška-Brezzi condition*,[22,23] which ensures the solvability of the linear matrix system in case of a saddlepoint problem, is not satisfied here thus unstable results occur.[19] Instead, mixed finite elements with higher order interpolation functions have to be used for the fluid regions, e.g. the so-called $Q_2 - P_1$ *Crouzeix-Raviart finite element*[21] with biquadratic polynomials for the displacement approximation and a linear, discontinuous approximation of the pressure including two derivatives. To ensure the continuity of the resulting displacement vector field, we also use *nine node quadrilateral finite elements* for rigid and elastic regions,

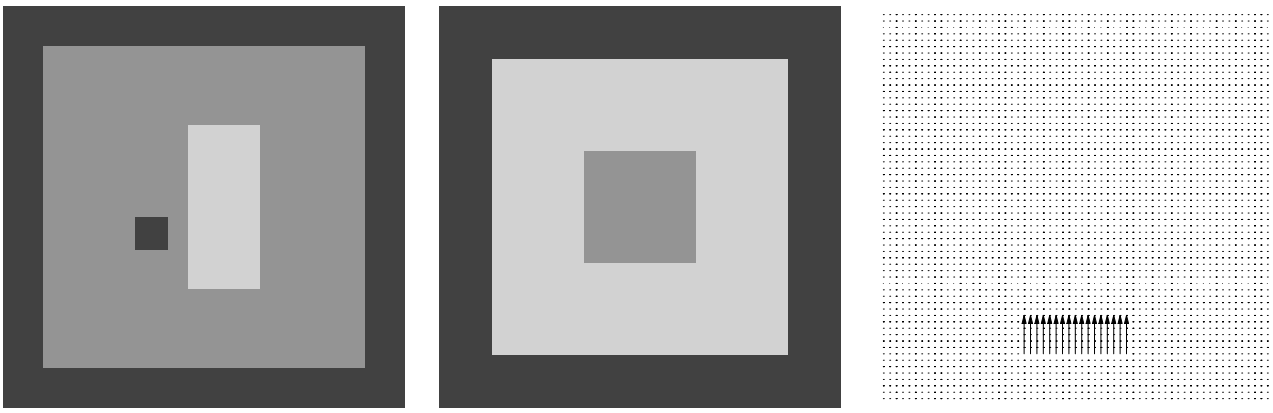

(a) (b) (c)

Figure 2. The synthetic images used in our experiments and the correspondences applied in the second experiment (see text).

though the usage of other types of finite elements with lower order interpolation functions seems possible. Problems arise with both types of finite elements due to the large number of associated degrees-of-freedom, which count to 21 resp. 18 per finite element in the 2D case, thus leading to large linear equation systems. Additionally, the $Q_2 - P_1$ Crouzeix-Raviart finite element prevents the usage of iterative solution techniques.[21] As a consequence, only images of relatively small size can be handled so far.

To calculate the deformation of an anatomical structure given prior defined spatial correspondences between images, these correspondences must be integrated into the linear equation system. To this end, we use the procedure described in Peckar *et al.*[25] and Huebner *et al.*.[26] Given a value for the unknown u_j, this can be incorporated into the linear equation system by a subtraction of the product $u_j \mathbf{A}_j$, where $\mathbf{A}_j$ denotes the j-th column of the stiffness matrix $\mathbf{A}$, from the righthand side vector $\mathbf{b}$, followed by a substitution of the given value into the j-th row of $\mathbf{b}$. Thereafter, the j-th row and column of $\mathbf{A}$ are set to zero and, respectively, the diagonal element A_{jj} to one. By repeating this procedure for a set of correspondences, to be given at the surface of an anatomical structure, a direct mapping from the undeformed to the deformed state of the anatomical structure results.

3. EXPERIMENTS

Our coupled rigid/elastic/fluid model has been tested on synthetic and tomographic images. For the experiments with the synthetic images shown in Figure 2 we model the following three different materials: rigid skull bone (black), cerebrospinal fluid (bright grey), and elastic brain tissue (dark grey). To assess the physical plausibility of our new model, we compared the results with those from our purely linear elastic model[5] assuming there at first a homogeneous elastic body only and, at second, an inhomogeneous elastic body with elastic brain tissue, rigid skull bone, and fluid treated as a rigid object. As mentioned above, this simulation of the fluid was motivated by the reported incompressibility of cerebrospinal fluid. In the following, we refer to these three approaches as *homogeneous elastic model*, *inhomogeneous elastic model*, and *inhomogeneous elastic/fluid model*, respectively. As material parameter values, we used the values determined in Hagemann *et al.*[5] for the Lamé constants and the heuristically determined value of 0.01 for the combined parameter $\mu^{\star} dt^{-1}$.

In the first experiment, we simulated the movement of a rigid object towards a nearby fluid region, using the synthetic image shown in Figure 2(a). The rigid object (small black square) may represent an instrument for surgery, a rigid foreign body, or a particle of skull bone. For simplicity, the movement is modeled as pure translation of the squared object using two parallel correspondences defined by $\mathbf{u} = (7.0, -4.0)^T$. We expect that the resulting deformation leads to a pure translation of the rigid object in the direction of the fluid region which should deform accordingly. As can be seen from the calculated results and the corresponding grid deformations in Figures 3(a) and (d), the homogeneous elastic model results in a deformation where both, the object and the surrounding skull bone were deformed which is in contrast to rigid material behavior. With the inhomogeneous elastic model this is not the case, but the assumed rigidity of fluid leads to physically incorrect violations of the grid topology as depicted in

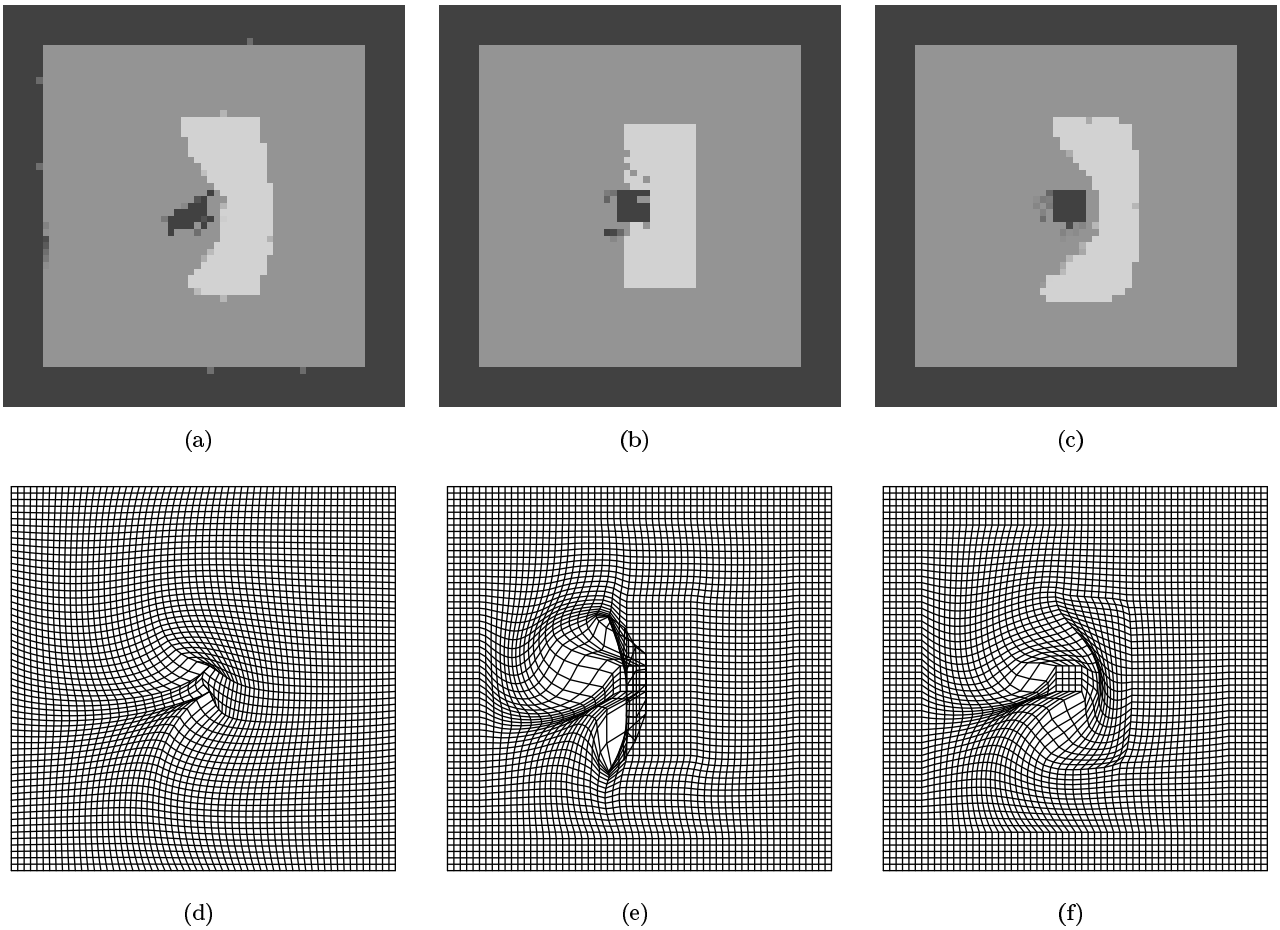

Figure 3. Calculated deformations for the synthetic image shown in Figure 2(a) (top row) and corresponding grid deformations (bottom row) using (a) a homogeneous elastic model, (b) an inhomogeneous elastic model, and (c) an inhomogeneous elastic/fluid model.

Figures 3(b) and (e). Additionally, no deformation occurs in the fluid region and the soft material between the object and fluid regions is no longer visible (note, that the rigid and elastic parts lie one above the other). A complete different behavior shows our inhomogeneous elastic/fluid model. Here, the shape of the rigid object is still preserved while the complete deformation takes place in the fluid and brain tissue regions, see Figures 3(c) and (f).

In the second experiment we simulated the growth of a tumor located inside a simulated skull bone by applying 17 parallel correspondences given by $\mathbf{u} = (0.0, -6.0)^T$ at the bottom part of the skull, as shown in Figure 2(c). We expect that, due to the incompressibility of the fluid and the rigidity of the surrounding bone, the elastic brain tissue will be compressed. As can be seen from Figure 4, the homogeneous elastic model leads to the worst result: no compression of the elastic part can be observed and even at the "rigid" bone deformations occur. Additionally, the assumed homogeneous Dirichlet boundary condition at the image boundaries lead to large and topology disturbing deformations in the rear of the given correspondences, see Figure 4(d). In contrast, the use of the inhomogeneous elastic model leads mainly to a deformation of brain tissue with some compression at the bottom part. Only our inhomogeneous elastic/fluid model gives the expected qualitative result. The brain tissue has been significantly compressed, as can be clearly seen in the corresponding grid deformation shown in Figure 4(f). Also, after a detailed analysis of the pixels belonging to each region, it turns out that the tumor enlargement is roughly equal to the shrinking of brain tissue.

For our experiment with a real tomographic image, we used the section of the preoperative MR image marked in Figure 5. The resulting image of size 61×61 pixels shows a part of the ventricular system surrounded by elastic brain tissue. In order to segment both regions, we applied a Canny edge detector to the image. Thereafter, the

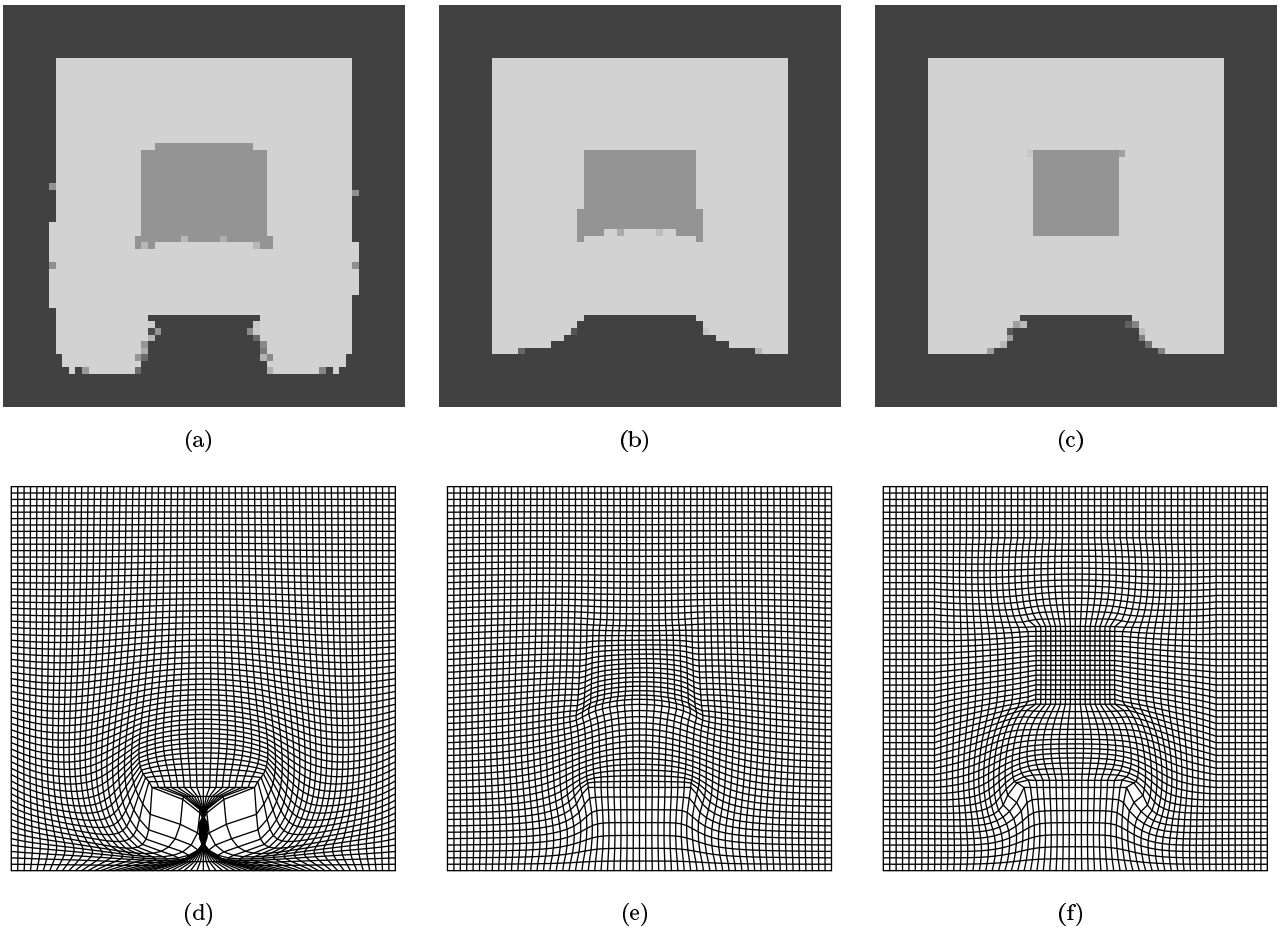

Figure 4. Calculated deformations for the synthetic image shown in Figure 2(b) (top row) and corresponding grid deformations (bottom row) using (a) a homogeneous elastic model, (b) an inhomogeneous elastic model, and (c) an inhomogeneous elastic/fluid model.

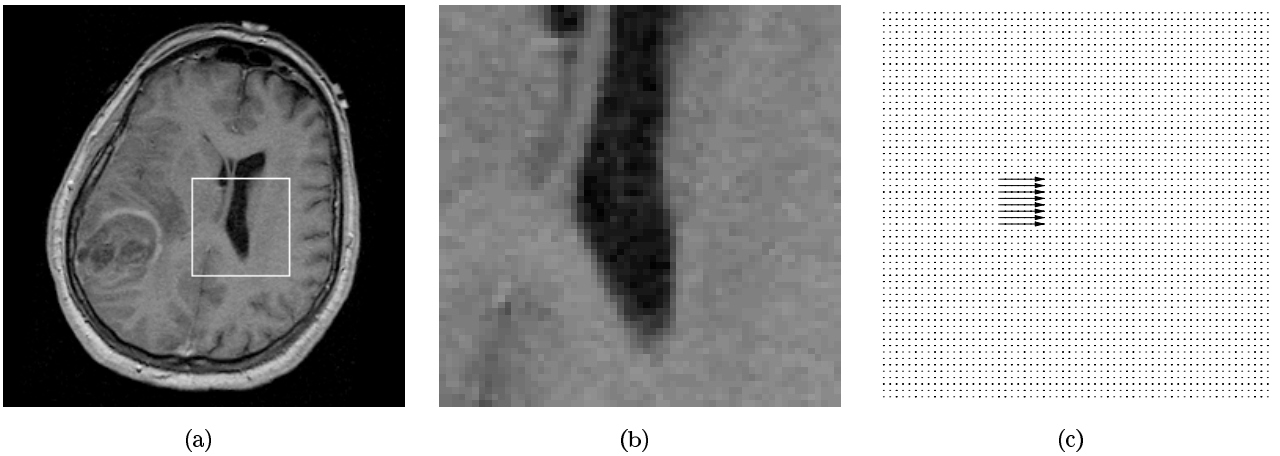

Figure 5. Enlarged part (b) of the ventricular system of the original preoperative image (a). The applied correspondences are depicted in (c).

resulting segmentation has been locally corrected such as to match the underlying finite element mesh. The final segmentation follows exactly the finite element boundaries.

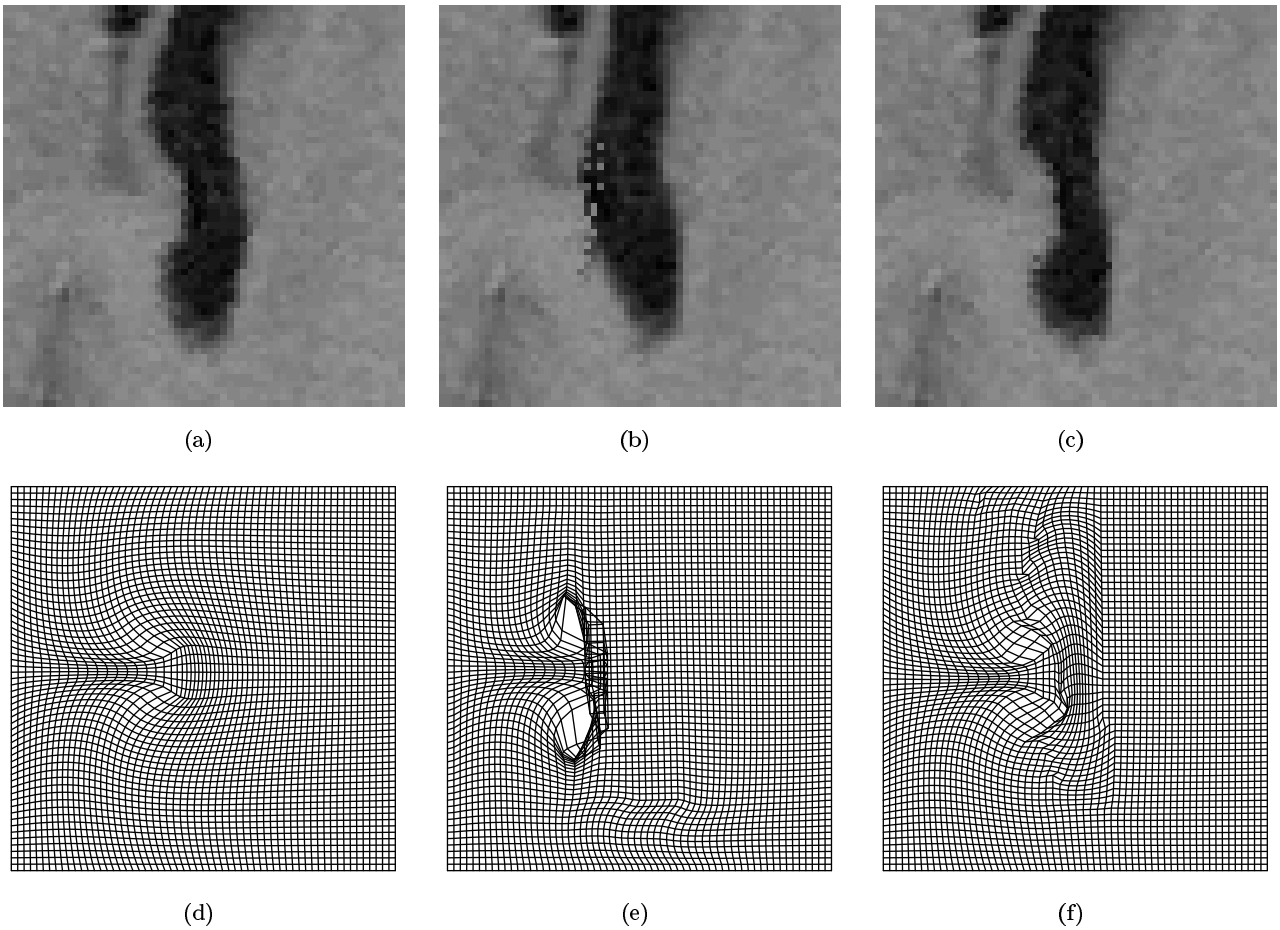

Figure 6. Resulting calculated deformations (top row) for the image in Figure 5(b) and corresponding grid deformations (bottom row) while using (a) a homogeneous elastic model, (b) an inhomogeneous elastic model, and (c) an inhomogeneous elastic/fluid model.

Figure 6 shows the results and corresponding grid deformations for 8 parallel correspondences (defined as $\mathbf{u} = (7.0, 0.0)^T$) given at the left side of the ventricular system, as shown in Figure 5(c). Using the homogeneous elastic model, a remarkably bended shape of the ventricular system results, see Figure 6(a). As indicated by the grid deformation in Figure 6(d) and the displacement vector field shown in Figure 7(a), this bending is symmetric with regard to the applied correspondences. Significant displacements occur in a rather local neighbourhood, i.e. no material flows to remote parts of the image. In contrast, the inhomogeneous elastic model leads to a corrupted and physically incorrect result according to a violation of the underlying topology, which is clearly visible in the grid deformation shown in Figure 6(e). As in the first experiment, such foldings sometimes occur in the vicinity of rigid structures due to large deformations at the boundary between an elastic and a rigid region (see also the corresponding displacement vector field in Figure 7(b)). Additionally, the shape of the ventricular system is nearly preserved thus indicating that the inhomogeneous elastic model is insufficient in this case.

Our inhomogeneous elastic/fluid model results in a completely different behaviour, see Figures 6(c) and (f). According to the shape of the enclosed fluid region, the predicted deformation is non-symmetric with regard to the given correspondences. Also, a clearly visible material flow inside the fluid region to the upper part of the image is visible. The result is a roughly straight right side of the ventricular system. Interestingly, the pressure of the fluid onto the brain tissue at the right side is nearly uniformly distributed as indicated by the resulting overall small displacements of the brain tissue there, see Figure 7(c).

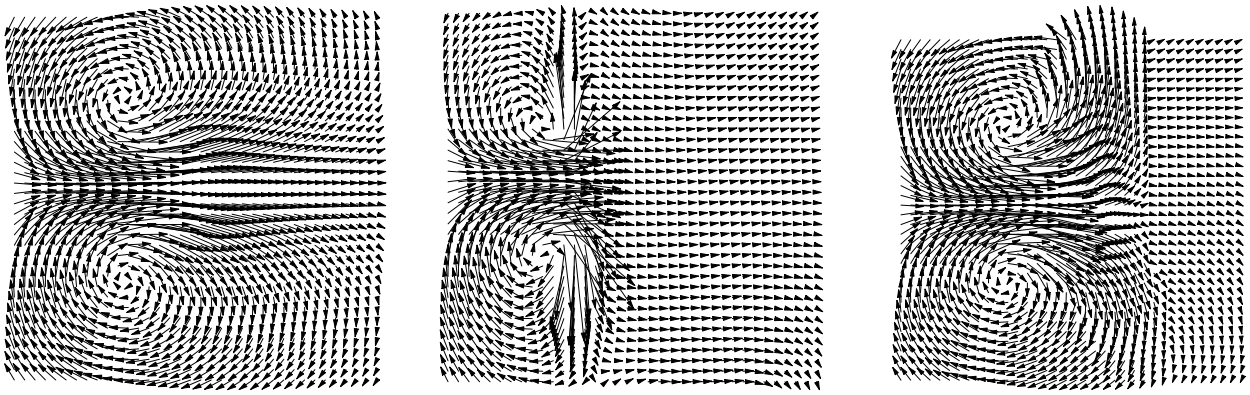

(a) (b) (c)

Figure 7. Parts of the calculated displacement vector fields for (a) the homogeneous elastic model, (b) the inhomogeneous elastic model, and (c) the inhomogeneous elastic/fluid model, respectively. The sections were taken from the middle of the images shown in Figures 6(a)-(c).

4. SUMMARY

We proposed a new biomechanical model of the human head for image correction purposes based on the finite element method. The model uses the physical theory of continuum mechanics to explicitly simulate the deformations of coupled rigid, elastic, and fluid regions. Instead of using forces, the deformation of the biomechanical model is driven by landmark correspondences. Experiments with synthetic as well as tomographic images have been carried out in order to assess the physical plausibility of the predicted deformation results. It turns out, that our new approach leads to a significant improvement of the predicted results compared to a pure linear elastic model. We expect that the incorporation of more advanced constitutive equations for brain tissue and other anatomical structures will further improve the results. Additional work will be carried out to reduce the size of the overall linear matrix system allowing to handle larger image sizes.

5. ACKNOWLEDGEMENT

Support of Philips Research Laboratories Hamburg, project IMAGINE (IMage- and Atlas-Guided Interventions in NEurosurgery), is gratefully acknowledged. Additionally, we thank Prof. Dr. med. J. M. Gilsbach and OA Dr. med. U. Spetzger of the Neurosurgical Clinic, Aachen University of Technology (RWTH) for providing us with the tomographic datasets used in the experiments.

REFERENCES

1. D. L. G. Hill, C. R. Maurer, R. J. Maciunas, J. A. Barwise, J. M. Fitzpatrick, and M. Y. Wang, "Measurement of Intraoperative Brain Surface Deformation under a Craniotomy," *Neurosurgery* **43**, pp. 514–526, September 1998.
2. R. D. Bucholz, D. D. Yeh, J. Trobaugh, L. L. McDurmont, C. Sturm, C. Baumann, J. M. Henderson, A. Levy, and P. Kessman, "The Correction of Stereotactic Inaccuracy Caused by Brain Shift Using an Intraoperative Ultrasound Device," in *Computer Vision, Virtual Reality and Robotics in Medicine and Medical Robotics and Computer-Assisted Surgery (CVRMed-MRCAS'97)*, J. Troccaz, E. Grimson, and R. Mösges, eds., vol. 1205 of *Lecture Notes in Computer Science*, pp. 459–466, Springer Verlag, (Grenoble, France), 1997.
3. P. J. Edwards, D. L. G. Hill, J. A. Little, and D. J. Hawkes, "Deformation for Image Guided Interventions Using a Three Component Tissue Model," in *Information Processing in Medical Imaging (IPMI'97)*, vol. 1230 of *Lecture Notes in Computer Science*, pp. 218–231, Springer Verlag, (Poultney, USA), June 1997.
4. O. Škrinjar, D. Spencer, and J. Duncan, "Brain Shift Modeling for Use in Neurosurgery," in *Medical Image Computing and Computer-Assisted Intervention (MICCAI'98)*, W. M. Wells, A. Colchester, and S. Delp, eds., no. 1496 in Lecture Notes in Computer Science, pp. 641–648, Springer Verlag, October 1998.

5. A. Hagemann, K. Rohr, H. S. Stiehl, U. Spetzger, and J. M. Gilsbach, "Nonrigid matching of tomographic images based on a biomechanical model of the human head," in *Medical Imaging 1999 – Image Processing (MI'99)*, K. Hanson, ed., Proceedings of the SPIE International Symposium, pp. 583–592, San Diego, USA, February 1999.
6. K. D. Paulsen, M. I. Miga, F. E. Kennedy, P. J. Hoopes, A. Hartov, and D. W. Roberts, "A Computational Model for Tracking Subsurface Tissue Deformation During Stereotactic Neurosurgery," *IEEE Transactions on Biomedical Engineering* **46**, pp. 213–225, February 1999.
7. C. Davatzikos, "Nonlinear Registration of Brain Images Using Deformable Models," in *Proceedings of the IEEE Workshop on Mathematical Methods in Biomedical Image Analysis*, M. E. Kavanaugh, ed., pp. 94–103, (San Francisco, USA), June 1996.
8. S. K. Kyriacou and C. Davatzikos, "A Biomechanical Model of Soft Tissue Deformation, with Applications to Non-rigid Registration of Brain Images with Tumor Pathology," in *Medical Image Computing and Computer-Assisted Intervention (MICCAI'98)*, W. M. Wells, A. Colchester, and S. Delp, eds., no. 1496 in Lecture Notes in Computer Science, pp. 531–538, Springer Verlag, October 1998.
9. H. Lester, S. R. Arridge, and K. M. Jansons, "Local deformation metrics and nonlinear registration using a fluid model with variable viscosity," in *Proceedings of the Medical Image Understanding and Analysis (MIUA'98), Leeds, UK*, E. Berry, D. Hogg, K. V. Mardia, and M. A. Smith, eds., pp. 44–48, University of Leeds, July 1998.
10. M. Ferrant, S. K. Warfield, C. R. G. Guttmann, R. V. Mulkern, F. A. Jolesz, and R. Kikinis, "3D Matching Using a Finite Element Based Elastic Deformation Model," in *Medical Image Computing and Computer-Assisted Intervention (MICCAI'99)*, C. Taylor and A. Colchester, eds., no. 1679 in Lecture Notes in Computer Science, pp. 202–209, Springer Verlag, September 1999.
11. K. B. Sahay, R. Mehrotra, U. Sachdeva, and A. K. Banerji, "Elastomechanical characterization of brain tissues," *Journal of Biomechanics* **25**, pp. 319–326, March 1992.
12. Y. Tada, T. Nagashima, and M. Takada, "Biomechanics of brain tissue (simulation of cerebrospinal fluid flow)," *JSME International Journal, Series A (Mechanics and Material Engineering)* **37**, pp. 188–194, April 1994.
13. G. E. Christensen, R. D. Rabbitt, and M. I. Miller, "Deformable templates using large deformation kinematics," *IEEE Transactions on Image Processing* **5**, pp. 1435–1447, October 1996.
14. A. Hagemann, K. Rohr, H. S. Stiehl, U. Spetzger, and J. M. Gilsbach, "Biomechanical modeling of the human head for physically-based, non-rigid image registration," *IEEE Transactions on Medical Imaging* **18**, pp. 875–884, October 1999.
15. Y. C. Fung, *Foundations of Solid Mechanics*, Prentice-Hall, 1965.
16. L. E. Malvern, *Introduction to the Mechanics of a Continuous Medium*, Prentice-Hall, 1969.
17. P. G. Ciarlet, *Mathematical Elasticity: Three-Dimensional Elasticity*, vol. 20 of *Studies in Mathematics and its Applications*, North-Holland, 1988.
18. P. J. Edwards, D. L. G. Hill, J. A. Little, and D. J. Hawkes, "A three-component deformation model for image-guided surgery," *Medical Image Analysis* **2**(4), pp. 355–367, 1998.
19. D. Braess, *Finite Elemente*, Springer Verlag, 1997.
20. Y. C. Fung, *A First Course In Continuum Mechanics*, Prentice-Hall, 1994.
21. C. Cuvelier, A. Segal, and A. A. van Steenhoven, *Finite Element Methods and Navier-Stokes Equations*, D. Reidel Publishing Company, 1986.
22. I. N. Bronstein and K. A. Semendjajew, *Teubner-Taschenbuch der Mathematik*, Teubner Verlag, 1996.
23. W. Hackbusch, *Theorie und Numerik elliptischer Differentialgleichungen*, Mathematik, Teubner Verlag, 1996.
24. H. Kardestuncer and D. H. Norrie, *Finite Element Handbook*, McGraw-Hill Company, 1987.
25. W. Peckar, C. Schnörr, K. Rohr, and H. S. Stiehl, "Parameter-free elastic deformation approach for 2-d and 3-d registration using prescribed displacements," *Journal of Mathematical Imaging and Vision* **10**, pp. 143–162, 1999.
26. K. H. Huebner, E. A. Thornton, and T. G. Byrom, *The Finite Element Method For Engineers*, John Wiley & Sons, 1995.